Macromolecules

pubs.acs.org/Macromolecules

Article

Cation–π Interactions Accelerate the Living Cationic Ring-Opening Polymerization of Unsaturated 2-Alkyl-2-oxazolines

Elias Van Den Broeck, Bart Verbraeken, Karen Dedecker, Pieter Cnudde, Louis Vanduyfhuys, Toon Verstraelen, Kristof Van Hecke, Valentin Victor Jerca, Saron Catak, Richard Hoogenboom,* and Veronique Van Speybroeck*

Cite This: *Macromolecules* 2020, 53, 3832–3846

Read Online

ACCESS | Metrics & More | Article Recommendations | Supporting Information

ABSTRACT: Cation–dipole interactions were previously shown to have a rate-enhancing effect on the cationic ring-opening polymerization (CROP) of 2-oxazolines bearing a side-chain ester functionality. In line with this, a similar rate enhancement—via intermolecular cation–π interactions—was anticipated to occur when π-bonds are introduced into the 2-oxazoline side-chains. Moreover, the incorporation of π-bonds allows for facile postfunctionalization of the resulting poly(2-oxazoline)s with double and triple bonds in the side-chains via various click reactions. Herein, a combined molecular modeling and experimental approach was used to study the CROP reaction rates of 2-oxazolines with side-chains having varying degrees of unsaturation and side-chain length. The presence of cation–π interactions and the influence of the degree of unsaturation were initially confirmed by means of regular molecular dynamics simulations on pentameric systems. Furthermore, a combination of enhanced molecular dynamics simulations, static calculations, and a thorough analysis of the noncovalent interactions was performed to unravel to what extent cation–π interactions alter the reaction kinetics. Additionally, the observed trends were confirmed also in the presence of acetonitrile as solvent, in which experimentally the polymerization is performed. Most intriguingly, we found only a limited effect on the intrinsic reaction kinetics of the CROP and a preorganization effect in the reactive complex region. The latter effect was established by the unsaturated side-chains and the cationic center through a complex interplay between cation–π, π–π, π–induced dipole, and cation–dipole interactions. These findings led us to propose a two-step mechanism comprised of an equilibration step and a CROP reaction step. The influence of the degree of unsaturation, through a preorganization effect, on the equilibration step was determined with the following trend for the polymerization rates: *n*-ButylOx < ButenOx < ButynOx ≥ PentynOx. The trend was experimentally confirmed by determining the polymerization rate constants.

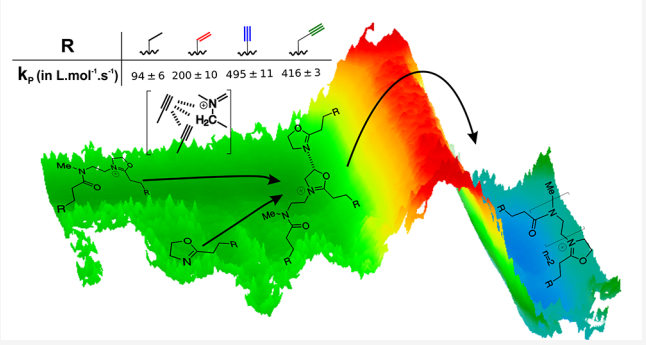

INTRODUCTION

The living cationic ring-opening polymerization (CROP) has long been known to provide wide access to poly(2-oxazoline)s with controlled end-group functionality.[1−9] Substituents on the 2-, 4-, and 5-positions can influence the propagation rates (k_p) significantly by electronic and/or steric effects, which govern the reaction (Scheme 1).[10−15] Despite their slow polymerization rates, 2-oxazolines substituted at the sp^3-hybridized carbons C_4 and C_5 can still be of interest as chemically inert ligands in organometallic chemistry or in asymmetric synthesis.[16−20] In contrast to the 4- and 5-substituted-2-oxazolines, 2-oxazolines substituted at the C_2 position provide access to a very interesting class of polymers: poly(2-alkyl/aryl-2-oxazoline)s (PAOx), which are biocompatible as well as thermosensitive and showed stealth behavior similar to poly(ethylene glycol) (PEG) and thus can be used in drug-delivery systems.[5,7,8,21,22]

Furthermore, the properties of PAOx are highly tunable by altering the C_2 substituent (see Scheme 1) of the monomer, which also enables introduction of (protected) side-chain functionalities.[7,11,23−26] Of particular interest in this study are 2-oxazoline monomers with alkene and alkyne functionalities, more specifically, 2-(but-3-enyl)-2-oxazoline (ButenOx, Scheme 1, **1b**), 2-(but-3-ynyl)-2-oxazoline (ButynOx, Scheme 1, **1c**), and 2-(pent-4-ynyl)-2-oxazoline (PentynOx, Scheme 1, **1d**). These functionalities are of interest for various click reactions, such as copper(I)-catalyzed azide cycloaddition as

Received: April 14, 2020
Published: May 4, 2020

Scheme 1. (Top) Schematic Representation of the Second Propagation Step in the Cationic Ring-Opening Polymerization (CROP) of 2-Oxazolines, Leading to the Formation of the Corresponding Trimer 3, Where *In* Is the Initiator Fragment at the Start of the Polymer Chain; (Bottom) 2-Oxazoline Structures for 2-(*n*-Butyl-2)-oxazoline (*n*-ButylOx, 1a), 2-(But-3-enyl)-2-oxazoline (ButenOx, 1b), 2-(But-3-ynyl)-2-oxazoline (ButynOx, 1c), 2-(Pent-4-ynyl)-2-oxazoline (PentynOx, 1d), 2-Difluorophenyl-2-oxazoline (*o*-DFPhOx, 1e), 2-Methoxycarbonylethyl-2-oxazoline (C_2-MestOx, 1f) 2-Methoxycarbonyl-propyl-2-oxazoline (C_3-MestOx, 1g)

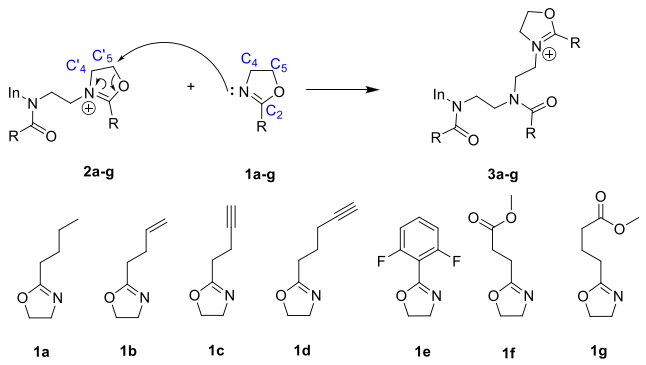

well as thiol−ene and thiol−yne reactions, which enable facile postfunctionalization of the resulting polymers. Click reactions on PAOx are typically performed by using copolymers and have found many practical applications, such as the introduction of targeting molecules on polymeric chains,[27] coatings of nanoparticles[28−31] or stainless steel,[31−33] creation of biocompatible materials with anode-selective deposition behavior,[33,34] and many others.[23,35−39] In addition, post-polymerization modification readily enables the introduction of side-chains that are not compatible with the CROP of 2-oxazolines.[40] Moreover, cross-linking of alkene- and/or alkyne-functionalized PAOx has been applied for the development of hydrogels or core−shell cross-linked nanoparticles.[22,25,41−43]

In general, the propagation rate constants for the CROP of 2-alkyl-2-oxazolines (Scheme 1) are governed by both electronic and steric effects, though the latter tends to have a more significant impact in most CROP reactions.[10,14] This effect explains the slower polymerization rates when increasing the alkyl chain from methyl up to propyl, with only marginal effects for longer side-chains.[14] Nonetheless, a few remarkable cases have been noted in the literature, some by the presenting authors, where electronic effects become prominent, particularly when functional groups or cyclic structures are introduced in the side-chain.[10−12,15,44,45] The use of a cyclic side-chain, such as *c*-propyl, was accompanied by an unexpected increase in propagation rate constant when compared to 2-oxazolines bearing its skeletal isomers, *i*-propyl and *n*-propyl.[10] This remarkable observation was theoretically rationalized by Goossens et al. using density functional theory (DFT) calculations, where the electronic effect of the cyclic side-chain in 2-*c*-propyl-2-oxazoline (*c*PrOx) was shown to become more significant during the CROP than the steric effect, which dominates in 2-*i*-propyl-2-oxazoline which was found to have a lower propagation rate constant than 2-*n*-propyl-2-oxazoline and *c*PrOx. This acceleration for the CROP of *c*PrOx was ascribed to the well-known (partial) π-bonding character of *c*-propyl carbons next to an imine.[10] The zwitterionic resonance structure shown in Scheme 2 is favored in the presence of this cyclic side-chain (through π-type

Scheme 2. Resonance Forms for *c*PrOx

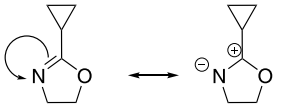

conjugation);[10] hence, the monomer's ability to perform a nucleophilic attack is significantly enhanced, positively influencing the reactivity of this S_N2-type reaction.

Another case in which electronic effects significantly influence the propagation rate constant was reported by Lobert et al. for the CROP of fluorinated and nonfluorinated analogues of 2-phenyl-2-oxazoline (PhOx).[15] When the phenyl side-chain and the 2-oxazoline ring are coplanar, the phenyl side-chain can withdraw electron density from the 2-oxazoline ring through conjugation; this effect is further enhanced when the phenyl ring is fluorinated. Hence, *meta-fluorinated* (*m*-FPhOx) and *para*-fluorinated PhOx (*p*-FPhOx) monomers have lower CROP rates than PhOx due to the decreased nucleophilicity of the monomer. However, *ortho*-substitution disrupts the conjugation by sterically preventing planarity (out-of-plane angle of 3°−4°). As a result, the electron-withdrawing effect of the fluoro-substituted phenyl side-chain is reduced to an inductive effect, which is much less effective than the electron-withdrawing effect through conjugation. Therefore, the propagation rate constant for *ortho*-monofluorinated PhOx (*o*-FPhOx) is significantly higher in comparison to the parent PhOx. In the 2-*o*-difluorophenyl-2-oxazoline system (Scheme 1, *o*-DFPhOx, **1e**), nonplanarity was further increased (out-of-plane angle of 39°), leading to a 2-fold increase of the propagation rate constant when compared to *o*-FPhOx. This latter effect was then confirmed by using MMFF94 calculations, which showed that in the case of *o*-DFPhOx there were two contributing factors. First, the steric clash caused by the *ortho*-fluorine substituent on the phenyl ring resulted in a nonplanar geometry with respect to the 2-oxazoline ring, effectively preventing conjugation, and as a result, the nucleophilicity of the 2-oxazoline was not significantly reduced. Second, a clear intermolecular interaction was shown to occur between the *ortho*-fluorine substituent and the cationic reaction center, which was hypothesized to increase the electrophilicity of the 2-oxazolinium cation, enhancing the CROP rates. Hence, this latter point indicates that dipole−cation interactions could also have a significant impact on the polymerization kinetics.

In view of prior studies that showed the varying effect of different side-chains on 2-oxazoline CROP propagation rate constants, Bouten et al. investigated the propagation rate constants of 2-oxazoline monomers with methyl ester substituents, namely, 2-methoxycarbonylethyl-2-oxazoline (Scheme 1, C_2-MestOx, **1f**) and 2-methoxycarbonylpropyl-2-oxazoline (Scheme 1, C_3-MestOx, **1g**).[11,12] Even though the propagation rate constants of the methyl ester-substituted 2-oxazolines were expected to be lower than their counterparts bearing aliphatic side-chains due to the electron-withdrawing ester functionality, faster propagation rate constants were experimentally observed. The authors rationalized these findings using DFT calculations, where they showed that the observed rate enhancement was mainly caused by the numerous inter- and intramolecular interactions between the

https://dx.doi.org/10.1021/acs.macromol.0c00865
Macromolecules 2020, 53, 3832−3846

carbonyl group of the side-chains and the active oxazolinium chain-end. The dipole−cation interaction between the carbonyl and the 2-oxazolinium moieties was shown to further increase the electrophilic nature of the chain-end, in particular, on the C_S' carbon atom, favoring nucleophilic attack (Scheme 1) and leading to the observed increase in CROP rate constants.

In the aforementioned studies, the CROP propagation rate constants of both *o*-DFPhOx[15] (Scheme 1, **1e**) and $C_{2/3}$-MestOx[11,12] (Scheme 1, **1f,g**) were increased by 2-oxazoline side-chains bearing electron-withdrawing groups (fluorine and carbonyl, respectively). The resulting intermolecular interaction between the electron-withdrawing species and the 2-oxazolinium chain-end further enhances both the electrophilic nature of the ring and the rate of the polymerization reaction. Both studies demonstrated that fine-tuning the side-chain of 2-oxazolines could induce rate-enhancing effects in CROP.

Based on this knowledge, a similar rate enhancement may be hypothesized when π-bonds are incorporated into 2-oxazoline side-chains, resulting in intermolecular cation−π interactions between the side-chain and the cationic chain-end, thereby potentially increasing their CROP rate constants. This hypothesis is proposed here for the first time and will be validated based on a combined experimental and molecular modeling study to investigate the CROP reaction rate constants of 2-oxazolines with side-chains of varying degrees of unsaturation (Scheme 1, monomers **1a−d**). The factors that affect the propagation rate constants were thoroughly examined by means of static DFT calculations and *ab initio* molecular dynamics simulations. We also tested the effect of the solvent on the specific interactions in the polymerization system. These computational predictions were further verified by an experimental kinetic study for monomers **1a−d** (Scheme 1) revealing that the computational evidence for cation−π interactions are translated into acceleration of the CROP of 2-oxazoline monomers with unsaturated side-chains. Despite the numerous previous reports on the CROP (co)polymerization of such monomers, this is the first in-depth study revealing faster polymerization resulting from cation−π interactions.

COMPUTATIONAL METHODOLOGY

In contrast to earlier modeling efforts, a multilevel modeling approach is applied in this study, where information about transition states is obtained from static DFT calculations while the conformational flexibility of the growing polymer chain is assessed from molecular dynamics studies. DFT-based simulations were performed on two types of model systems for each monomer **1a−d** (Scheme 1): a pentameric system, to monitor the presence and persistence of cation−π interactions, and a trimeric system, to compare the intrinsic reactivity of the monomers toward CROP monomer addition reactions.

Static Calculations. To compare the relative activation barriers for the prototypical CROP propagation step depicted in Scheme 1, a series of static calculations were performed on 2-oxazoline monomers **1a−d**. Methyl is taken as initiator fragment for the CROP in the systems under investigation, which is in accordance with the frequent use of methyl tosylate and methyl triflate as initiator in experimental studies. The B3LYP/6-311+G(d,p) level of theory was used for geometry optimizations to which Grimme's D3 dispersion corrections were added to take into account noncovalent and long-range interactions.[46] This functional has been proven to give reliable results for similar systems.[47−50] Normal-mode analysis was used to characterize the nature of the energetic minima and first-order saddle points (transition states (TSs)). To generate a representative set of reactant complexes, intrinsic reaction coordinate calculations are performed for a limited number of TSs.[51−53] Additionally, the solvent effects on the obtained complexes are assessed by using the integral equation formalism variant of the polarized continuum model (IEF-PCM).[54] All static calculations were performed using the Gaussian 16 package.[55] TS guesses were generated by using enhanced sampling simulations, namely metadynamics, which provided a critical distance for the TS region and sufficient sampling to explore the conformational flexibility of the TSs (see Supporting Information section S1.1).[56]

Molecular Dynamics Simulations. The CP2K software package[57] was utilized to carry out nonperiodic molecular dynamics (MD) simulations. The BLYP functional along with additional Grimme D3 dispersion corrections and the TZVP-GTH basis set were used to perform *ab initio* MD.[46,57−60] Given the extensive number of first-principles molecular dynamics simulations that were performed, it was impossible to use the hybrid B3LYP functional in view of computational time. However, the BLYP functional has shown to give a reasonable description of noncovalent interactions when D3 corrections are included with comparable performance to dispersion corrected hybrid functionals such as B3LYP-D3.[61] This basis set is a combination of Gaussian basis functions and plane waves (GPW) with a cutoff energy of 320 Ry.[62,63] The equations of motion were integrated with a time step of 0.5 fs. All systems were simulated by using the canonical ensemble at 413 K, which is controlled by a Nosé−Hoover thermostat chain of length five.[64,65] The pentameric ButylOx, ButenOx, and ButynOx were simulated by using a cubic box of 29 Å × 29 Å × 29 Å. For the pentameric PentynOx a box size of 33 Å was used. The solvent environment (acetonitrile) and the counterion (tosylate or triflate) were not considered in these first-principles MD-based simulations as this would require the simulations of a complete explicit solvent shell and would become computationally unfeasible. Emenike and co-workers have shown, by the use of molecular balances, that free energy differences for similar noncovalent interactions in the gas phase may be overestimated but in general are within the context of the values in solution, i.a., for acetonitrile.[66,67] Furthermore, cation−π interactions among other interactions were shown to prevail in acetonitrile by other experimental groups, which is in line with the theoretical work reported by Dougherty et al.[68−71] To verify our findings and this assumption, the density-functional tight binding (DFTB) method implemented in CP2K (enabling dispersion corrections; an Ewald-type method for Coulomb interactions and the self-consistent field method) is used to perform semiempirical MD simulations (see Supporting Information section S2.2.3) which allow us to investigate the influence of an explicit solvent environment in a computational efficient manner (*vide infra*).[72−76]

To achieve a sufficient sampling of the phase space for the *ab initio MD*, the system was first equilibrated for 10 ps followed by a production run of 100 ps. For each system, three separate simulations were run in parallel with three different initial geometries. More specifically, a folded, an extended, and a random coil conformation were used for each pentameric system to consider the flexibility of the chain. Initially, the presence of cation−π interactions was determined by analyzing the evolution of the distances of the penultimate side-chain bonds toward the cationic center with a cutoff distance of 4 Å,

https://dx.doi.org/10.1021/acs.macromol.0c00865
Macromolecules 2020, 53, 3832−3846

well-known as the optimal distance for these types of interactions.[77,78]

To further analyze and compare the MD results of the different systems, and thus elaborate on the strength of the interaction with the cationic center, the sampled phase space for the side-chains attached to the oxazolinium moiety was divided into two distinct regions depending on the proximity of the terminal side-chain bond to the cationic center (see Supporting Information section S2.1.2 and Figure S7). The distribution of the interaction distances allows the selection of two interfaces for each system, which enables a division into two different states: one "interacting" and one "noninteracting".[79,80] If a conformation is located in between these interfaces, the state will be classified as "interacting" if its previous conformation was classified as "interacting", and vice versa. This methodology was adopted from Van Erp and coworkers.[81] The relative strength of the cation−π interaction (or cation-induced dipole in the case of ButylOx) is evaluated through the mean distance between the side-chain terminal bond and the cationic ring attained in the interacting state. To explicitly test the effect of the acetonitrile solvent, this procedure was also conducted at the DFTB level of theory (see Supporting Information section S2.2.3.1).

Umbrella Sampling Simulations. Because the CROP propagation step is an activated process, it would not be observed within a regular MD simulation within a reasonable simulation time. Hence, we performed enhanced sampling molecular dynamics as well. More specifically, a series of gas-phase umbrella samplings were performed to determine the free energy profile for the second propagation step of the CROP.[82]

In the umbrella sampling (US) method the reaction coordinate is subdivided into a number of windows along the proposed reaction coordinate q. For the CROP reaction, the collective variable (CV) of choice was defined as the difference between distances of the breaking and the forming bonds: d(C−N) − d(C−O) (as schematically shown in Scheme 3).[83,84] By the selection of a proper CV, which uniquely describes the reaction coordinate q, US simulations could be used to sample specific regions of the free energy surface. The reactant and product regions are described by CV values higher than 0.1 and lower than −0.1, respectively.

Scheme 3. Collective Variable for the CROP Reaction

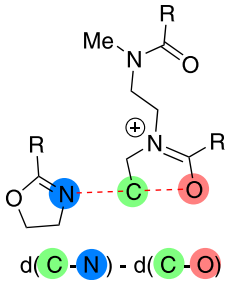

The CP2K software was used as the MD engine and interfaced with the PLUMED module to perform the US simulations.[85,86] For each system, umbrellas were placed along the CV from −2.8 to 3.2 Å with an increment of 0.1 Å, hence 59 windows. For each of these windows a biased MD simulation is performed. Initial configurations for each window were randomly selected from a moving bias potential simulation, which encapsulates the entire reaction coordinate region of interest. Sufficient sampling was ensured by employing harmonic bias potentials centered around the equilibrium value q_0 and with bias spring constant κ.

$$U_b(q) = \frac{\kappa}{2}(q - q_0)^2$$

The κ value was chosen at 250 kJ mol^{-1} Å^{-2}. Furthermore, in a second phase, the CV range was extended to 5.4 Å by placing an extra 10 windows with an increment of 0.2 Å and a κ value of 100 kJ mol^{-1} Å^{-2} to explore the reactant region more extensively. Subsequently, the free energy profiles were reconstructed by combining the sampled collective variable distribution in each window by using the weighted histogram analysis method (WHAM).[87−89] To extract Helmholtz free energies of activation from these profiles and kinetic data (using additional trajectory information about the US simulations), a method based on transition state theory is used which was applied by our research group before.[90] Assessment of convergence for the obtained profiles has been performed using the bootstrap method (see the Supporting Information).

Furthermore, the constructed 1D free energy profiles are transformed into 2D free energy surfaces (see Supporting Information section S1.3) with newly proposed collective variables based on the noncovalent interaction analysis (*vide infra*), e.g., the distance between the side-chain terminal bonds and the oxazolinium ion or the distance between the attacking monomer side-chain terminal bond and those of the growing polymer. This was done to analyze both the broadness of the various regions and the effect of noncovalent interactions hereon.

To assess the effect of the solvent environment on the prereactive complex region, umbrella sampling simulations are performed to constrain the system within the prereactive complex region. Hence, umbrellas were placed along the CV range of this prereactive region (from 0.0 to 10.5 Å) with an increment of 0.5 Å and a κ value of 100 kJ mol^{-1} Å^{-2} resulting in 20 windows. The results are discussed in the Overall Reactivity Pattern section (*vide infra*) and section S.2.2.3.2 of the Supporting Information.

Noncovalent Interactions Analysis. Analysis of intermolecular interactions was performed using the Non-Covalent Interaction (NCI) index plot tool, NCIPLOT (see Supporting Information section S1.2).[91,92] A cutoff for both the reduced gradient and the electron density is required to visualize specific interactions and discriminate between them. These were selected based on the graph of the reduced gradient in function of the electron density ($\rho(\mathbf{r})$, multiplied with the sign of λ_2) produced by NCIPLOT. This allowed for a more specific determination of the optimal plotting cutoff to capture and distinguish the different important interactions for each transition state. A typical cutoff for the systems under investigation is 0.025 for the electron density and 0.3 for the reduced gradient.

RESULTS AND DISCUSSION

Theoretical Results. To investigate the effect of introducing unsaturated side-chains to 2-oxazolines on the CROP, four different monomers with side-chains of varying degrees of unsaturation were chosen (Scheme 1, monomers **1a**−**d**), covering a saturated side-chain (**1a**), double (**1b**) and triple bonds (**1c** and **1d**), and a change in the distance between the triple bond and the 2-oxazoline ring. The presence/

https://dx.doi.org/10.1021/acs.macromol.0c00865
Macromolecules 2020, 53, 3832−3846

absence of cation−π interactions between the unsaturated side-chains and the cationic chain-end were investigated via regular MD simulations that were performed on pentameric systems of each monomer. Subsequently, the influence of the cation−π interaction on the propagation rate constant was explored by modeling the second propagation step (the formation of a trimeric chain) of the CROP reaction for **1a−d** by using both static DFT calculations to map the reaction free energy profile as well as enhanced sampling *ab initio* techniques to sample the broadness of the conformational space in both the reactant and transition state region. In the first instance, the simulation results were thoroughly and comparatively analyzed for all four systems to elucidate differences in their reactivity, indeed revealing evidence for cation−π interactions. In the second instance, the computational hypothesis was confirmed experimentally. To this end, the monomers **1a−d** were synthesized, and their CROP propagation rate constants were experimentally determined in an effort to validate the computational predictions for the relative CROP reaction rates.

Cation−π Interactions: Evidence from Regular Ab Initio MD Simulations. In the aforementioned study by Bouten et al., a semiempirical MD simulation on a decameric C_2-MestOx system (Scheme 1, **1f**) demonstrated the consistent presence of cation−dipole interactions between the side-chain carbonyl moieties and the 2-oxazolinium chain-end.[11] To investigate the proximity of the side-chain-ends of the pentameric chains from monomers **1a−d** shown in Scheme 4, the distance of the first side-chain up to the fifth side-chain, marked as s1 to s5, respectively, to the cationic center marked in yellow was followed. Additionally, the proximity of the carbonyl moieties was also investigated (marked in green in Scheme 4). If a distinct difference between the simulations for the systems with the unsaturated side-chains, namely pentaButenOx, pentaButynOx, and pentaPentynOx, and the reference system bearing a saturated butyl side-chain, pentaButylOx, is observed, this will serve as an indicator of the presence of cation−π interactions. Furthermore, these simulations will help shed light on the influence of both the degree of unsaturation and the proximity of the unsaturated terminal bond on the occurrence of cation−π interactions.

Scheme 4. Pentameric Chains with Side-Chains of Differing Degrees of Unsaturation: PentaButylOx (a), PentaButenOx (b), PentaButynOx (c), and PentaPentynOx (d)[a]

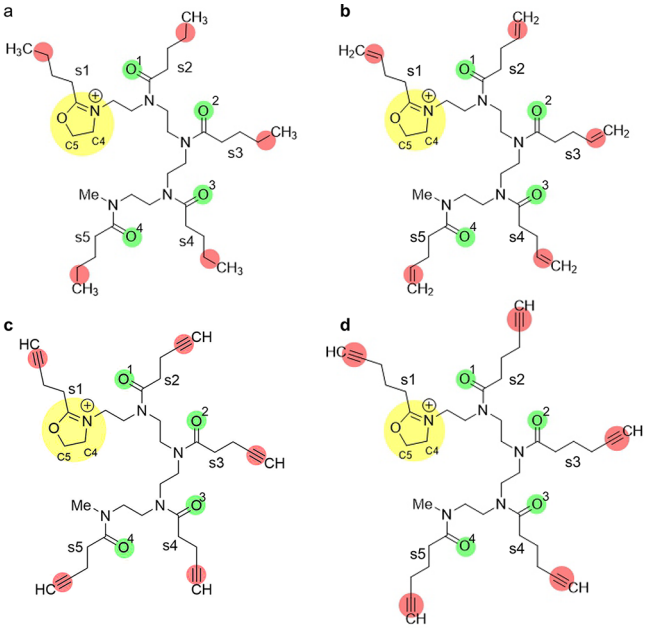

[a]Cationic chain-ends, backbone carbonyl groups, and side-chain terminal groups are shown in yellow, green, and red, respectively. s1−s5 and O^1−O^4 refer to side-chains 1−5 and carbonyl groups 1−4, respectively.

Figure 1 shows the time evolution of the distance between the side-chain terminal bonds and the cationic chain-end for each system (a complete overview of all regular MD results is found in the Supporting Information, Figures S2−S5). The MD results show a clear correlation between the degree of unsaturation and the extent of interactions occurring between the side-chain terminal bonds and the center of the 2-oxazolinium moiety. For the pentaButylOx system (Figure 1a), as anticipated, no specific interaction was observed between the side-chains and the cationic center. However, for pentaButenOx, pentaButynOx, and pentaPentynOx, simulations clearly show consistent proximity (~4 Å) between the side-chain terminal groups and the 2-oxazolinium chain-end throughout the simulation (Figure 1b−d). In most instances, multiple side-chains were shown to interact with the 2-oxazolinium cation, which was further verified through the orientation and proximity of the side-chains in the snapshots shown for each system (Figure 1, snapshots represent the interactions in the time span of the rectangular region). It should also be noted that regardless of the substituent's nature, the side-chains occasionally come relatively close to the cationic center due to cation−dipole (carbonyl) interactions, which are present in all systems. These interactions cause a prominent folded conformation in all pentameric structures (see section S2.1.1 and Figures S2−S5 in the Supporting Information).

To evaluate the relative strength of the cation−π interaction for the different systems, distinct "interacting" and "non-interacting" states are defined for the side-chain terminal bond attached to the oxazolinium ion for which the mean distance within the former state will act as an indicator for the corresponding interaction strength, as previously explained in the Methodology section, allowing to distinguish each interaction between the side-chain and the cationic chain-end. Note that this side-chain (Scheme 4, s1) is always in close proximity to the cationic center due to its connectivity, and in the case of pentaButylOx, a cation-induced dipole interaction with the chain-end is always possible, albeit significantly weaker and less persistent than a cation−π interaction. In contrast to pentaButylOx, the systems bearing unsaturated side-chains exhibited distinct "interacting" states between their side-chain terminal bond and their 2-oxazolinium centers (see section S2.1.2 and Figure S7 of the Supporting Information), giving further evidence for the occurrence of "cation−π" interactions. Furthermore, the influence of the degree of unsaturation is clear from the mean interaction distance, which decreases from 4.39 Å for ButylOx to 4.11, 4.07, and 3.59 Å for ButenOx, ButynOx, and PentynOx, respectively. This decrease in mean interaction distance reflects the increase in interaction strength between the side-chain terminal bonds and the cationic center (from cation-induced dipole to cation−π interactions). Although the interaction distance for ButynOx only slightly decreases with respect to ButenOx, we anticipate this interaction to be significantly stronger as it is hampered by

https://dx.doi.org/10.1021/acs.macromol.0c00865
Macromolecules 2020, 53, 3832−3846

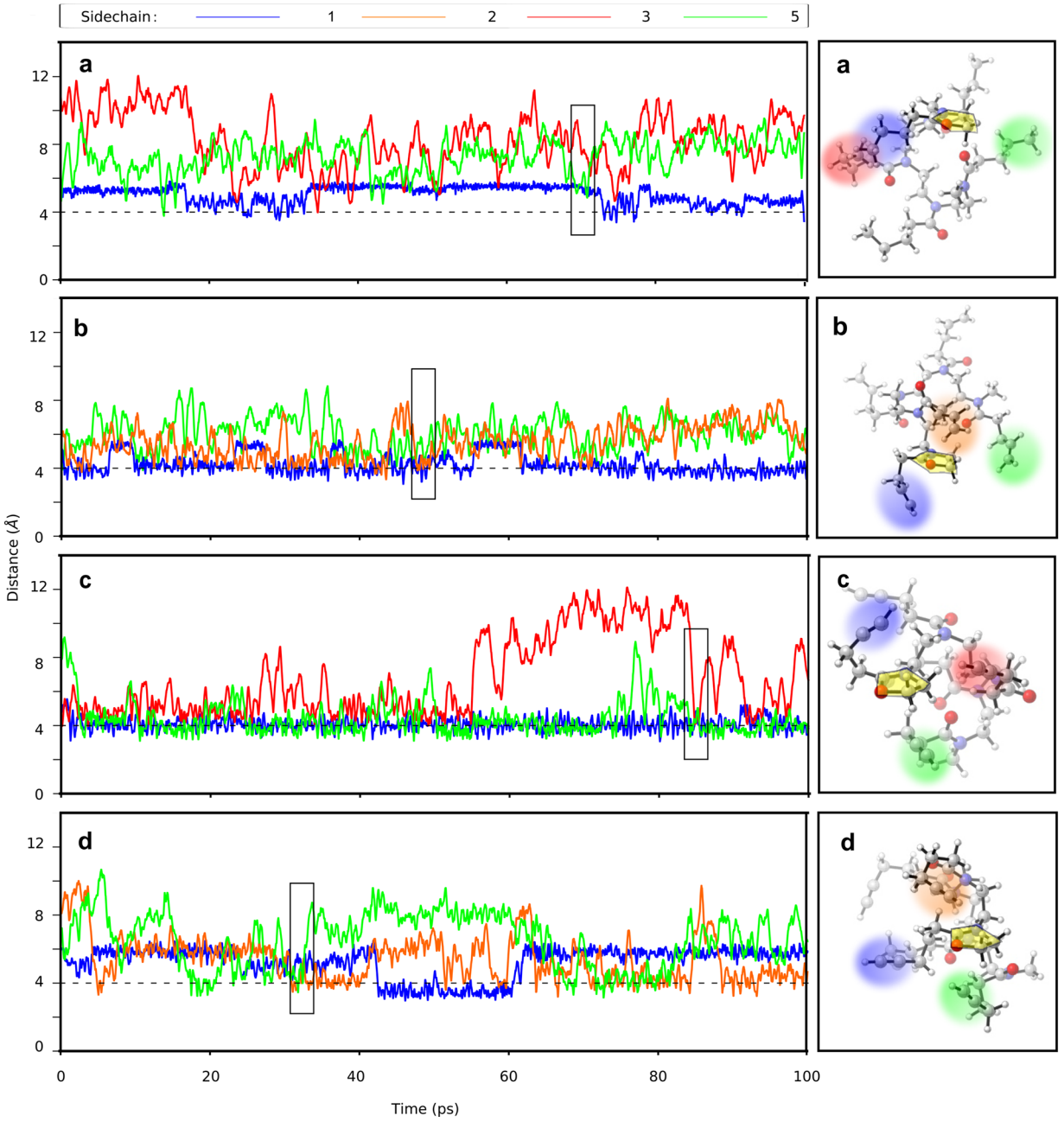

Figure 1. Evolution of distances for a representative MD run between the side-chain terminal bonds and the center of the 2-oxazolinium end-group (colored in yellow in the right panels) for pentaButylOx (a), pentaButenOx (b), pentaButynOx (c), and pentaPentynOx (d). Snapshots (right-hand side) indicate the interaction pattern observed in the rectangular region time span for each system; color codes shown at the top (see Supporting Information section S2.1 for all the results).

steric constraints for its shorter "arm-like" side-chain with respect to PentynOx, which does show this increase in strength. Additionally, comparison of the ButynOx and PentynOx simulations (see section S2.1 as well as Figures S4, S5, and S7 of the Supporting Information) suggests an entropic penalty for the pentyn side-chains, as the interacting state is less prominent in comparison to ButynOx.

In conclusion, the regular first-principles MD simulations provide evidence for the occurrence of favorable cation−π interactions between unsaturated side-chains and the cationic 2-oxazolinium chain-end. In the next section, the intrinsic reaction kinetics will be studied for a trimeric model system to investigate whether these cation−π interactions will also affect the reaction kinetics. We also evaluated whether these interactions are preserved in the presence of acetonitrile, which was indeed the case (section S.2.2.3 of the Supporting Information).

Reactivity and Energetics: Static DFT vs Enhanced Sampling Ab Initio Dynamics Calculations. The present study aims to elucidate the effect that cation−π interactions may have on the CROP propagation rate constants. However, it is important to first distinguish whether these monomers may have different intrinsic reactivity resulting from the different electronic nature of their side-chains. For this purpose, smaller dimeric model systems (Scheme 5) were

https://dx.doi.org/10.1021/acs.macromol.0c00865
Macromolecules 2020, 53, 3832−3846

chosen to determine the activation barrier for the second propagation step of the CROP propagation reaction.

Scheme 5. Schematic Representation of Trimeric Model System Used in the Second Propagation Step of CROP

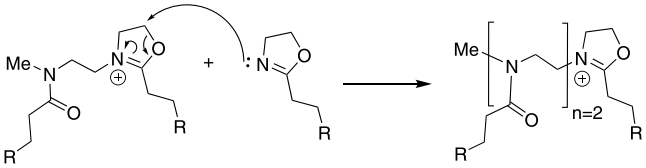

As the systems under study are extremely flexible, we opted to initially explore the transition state region by metadynamics simulations. From these simulations a representative set of transition states were extracted that were further optimized by using static DFT calculations. Relevant states were selected based on a critical distance; more information is provided in Supporting Information section S1.1. For each of the systems **1a−d** in Scheme 1, about 70−90 transition states were identified by using this procedure. A summary of all reaction barriers for each of these states is given in Supporting Information section S2.2 and Tables S1−S4. All conformers are shown with respect to their corresponding separate reactant in which the unfolded conformer of the dimer is taken for comparability. The highly variable range of transition state free energies and conformers emphasizes both the complexity and the multidimensionality of the free energy surface due to the many degrees of freedom (DoF). A summary of the obtained free energy barriers and separate enthalpic and entropic contributions are visually shown in Figure 2. Some transition states that are expected to control the minimal free energy path connecting the separate reactants and the trimer are indicated by **a1**, **b1**/**b2**, **c1**, and **d1** in Figure 2 for *n*-ButylOx, ButenOx, ButynOx, and Pentynox, respectively. The corresponding free energy barriers reveal the following trend *n*-ButylOx > ButenOx > ButynOx ≤ PentynOx with a difference of <5 kJ mol^{-1} between ButynOx and PentynOx. It is important to note that the values here correspond to separate reactants and that the observed effect of the side-chain could be originating from the preorganization effect in which the side-chain has preferable interactions with the reacting center or from the intrinsic reaction kinetics. For ButenOx, including an unsaturation in the side-chain mainly enables extra enthalpic stabilization with respect to the saturated side-chains for *n*-ButylOx. This yields an extra stabilization of the ButenOx transition states lowering the activation barrier by 12.6 kJ mol^{-1} with respect to *n*-ButylOx. Increasing the degree of unsaturation from a double to a triple bond, i.e., from ButenOx to ButynOx, a further enthalpic stabilization effect is observed with a change in Gibbs free energy of 12.3 kJ mol^{-1} with respect to ButenOx. However, the most stable transition states for ButynOx, on average, show higher entropic barriers with respect to ButenOx which can be explained by the more rigid-arm-like (sp-hybridized) structure of the butynyl side-chain showing less flexibility than the butenyl side-chain (*vide infra*). For the PentynOx system, a higher entropic penalty is also observed, and thus, the overall reaction kinetics may be expected to be lower compared to the Butynox system. This balance between enthalpic and entropic effects causes the free energies of the controlling TSs of PentynOx to be slightly higher than for ButynOx with a difference in ΔG of 3.8 kJ mol^{-1}. The higher entropic dependence for PentynOx thus confirms the suggestion for the entropic penalty for the pentyn side-chains (*vide supra*). Hence, the influence of both the degree of unsaturation and

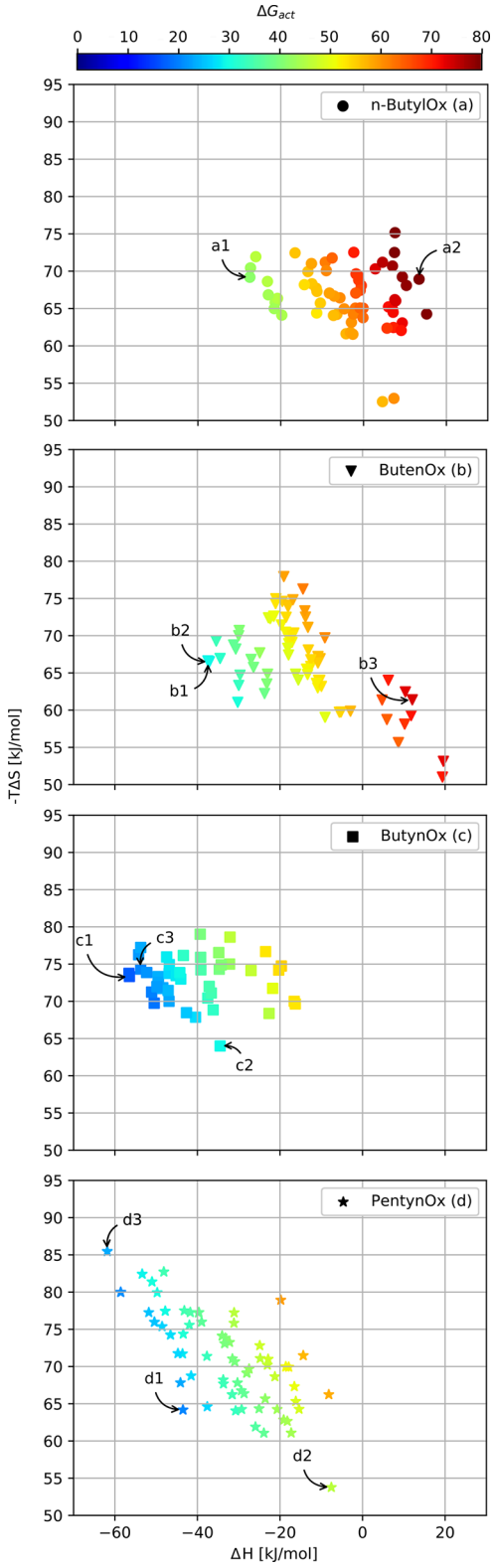

Figure 2. Optimized transition states for the systems under investigation (B3LYP-D3/6-311+G(d,p), 298 K, in vacuum). Entropy and enthalpy with respect to the separate reactants with the unfolded dimer as a reference.

https://dx.doi.org/10.1021/acs.macromol.0c00865
Macromolecules 2020, 53, 3832−3846

the side-chain length is shown to exist, indicating the possible positive effect of the cation−π interaction on the Gibbs free activation barriers. To obtain more insight into the inter- and intramolecular interactions at play in the various TSs, an extensive analysis was performed using the NCI-plot tool.[91]

Intra- and Intermolecular Interactions. Because the most important differences between *n*-ButylOx, ButenOx, and ButynOx systems are the enthalpic contributions (based on Figure 2), we explored which interactions are causing this extra stabilization and, hence, find the controlling inter- and intramolecular interactions for the CROP reaction of the respective systems. In Figure 3, the NCI plots for the most

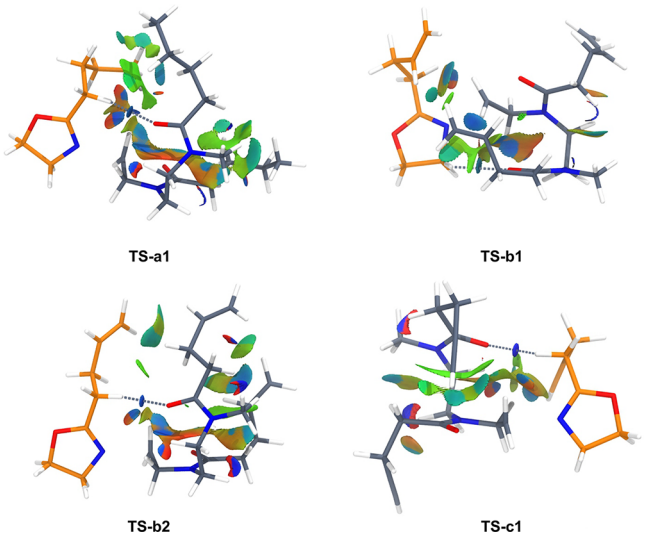

Figure 3. NCI plots of the selected transition state structures for the propagation reaction of ButylOx (**a**), ButenOx (**b**), and ButynOx (**c**) (see Figures S16−S19 for multiple viewpoints of **a**, **b**, **c**, and PentynOx (**d**)). The attacking monomer is displayed in orange and the growing polymer in gray. The 2-oxazolinium ring is opening (C- -O) due to the attack of the nitrogen atom. The blue surfaces indicate stabilizing interactions, the green surface indicates van der Waals interactions, and the red surface typically indicates steric hindrance. The dotted line between the attacking monomer and growing polymer represents a stabilizing dipole−induced dipole interaction.

stable (lowest Gibbs free energy) TS conformations are shown for the formation of triButylOx, triButenOx, and triButynOx, which were discussed in the previous section (*vide supra*). The PentynOx system is discussed in Supporting Information section S2.1.1 as well as the other transition states indicated in Figure 2.

For the propagation reaction resulting in triButylOx, **TS-a1** shows interactions between the carbonyl moiety of the amide ($CH_3NHC{=}O$) and the 2-oxazolinium carbon atoms (OCH_2CH_2N) as indicated by the blue surfaces in between these moieties. This is in line with the finding for the pentameric systems (see section S2.1.1 and Figures S2−S5) and previous work by Bouten et al. for methyl ester-functionalized 2-oxazoline monomers.[11,12] This interaction is also observed for the other systems and will hence not be responsible for the extra stabilization effect present in the unsaturated systems (see Figure 3, section S2.2.1, and Figures S9−S12). Structure **TS-a1** (Figure 3) shows that for triButylOx no significant stabilizing interactions (which would be indicated in blue) are present between the polymer side-chains and the reactive center of the 2-oxazolinium. However, stabilizing interactions are observed between the attacking monomer side-chain and both the carbonyl moiety (a dipole−induced dipole interaction indicated by the dotted line and blue surface perpendicular to it between $NCC\mathbf{H}_2$ and $C{=}\mathbf{O}$) and the terminal side-chain of the dimer (indicated by blue/green surfaces between the orange and gray side-chains) which is ascribed to a preorganization effect. It is anticipated that this effect will be stronger or more pronounced in the case of unsaturated side-chains.

For triButenOx both **TS-b1** and **TS-b2** are shown in Figure 3 because the interactions present will dominate the transition state landscape and can be compared to triButylOx to investigate the effect of the unsaturation in the side-chain. However, their conformations are very different with respect to each other and, connected with this, so are the dominating NCI. In contrast to **TS-a1**, a clear stabilizing interaction occurs between the unsaturated moiety of the growing polymer and the 2-oxazolinium moiety for **TS-b1** (indicated by a blue surface between $\mathbf{CH_2{=}CH}$ and $CH_2\mathbf{CH_2}N$), which is the anticipated cation−π interaction. Additional stabilizing cation−π interactions are present between the attacking monomer side-chain and the 2-oxazolinium ($\mathbf{CH_2{=}CH}$ and $CH_2\mathbf{CH_2}O$). This latter interaction indicates again the presence of a preorganization effect between the attacking monomer and the growing polymer. Remarkably, this TS dominated by cation−π interactions is equally favorable than **TS-b2**, which is not showing any cation−π interactions. **TS-b2** is dominated by both π−π and π-induced dipole ($\mathbf{CH_2{=}CH}$ and $CH\mathbf{CH_2}CH_2$) interactions between the side-chains, causing enthalpic stabilization equal to the cation−π interactions observed for **TS-b1** (see Figure 2). These latter interactions can again be ascribed to a preorganization effect that is present between the monomer and the growing polymer, which, hence, is stronger than the effect present in **TS-a1** (based on the enthalpic stability see Figure 2). For the CROP of ButynOx, similar conclusions can be made for **TS-c1** and **TS-c3** (see Figure 3, section 2.2.1, and Figure S10) as was done for **TS-b1** and **TS-b2**. Hence, the most important results from the NCI analysis are that, on one hand, the governing inter- and intramolecular interactions show different patterns and indicate that unsaturations in the side-chains give access to a range of interactions providing extra enthalpic stabilization and, on the other hand, that cation−π, π−π, dipole−induced dipole, and π-induced dipole interactions are present between the attacking monomer and the growing polymer, indicating an important preorganization effect in all investigated systems.

In summary, these results indicate that the difference in the Gibbs free energy of the investigated systems can be ascribed to the degree of unsaturation and their corresponding interaction patterns. Furthermore, it is found that cation−π interactions are not solely responsible for stabilizing the TS structures but that it is rather a combination of cation−π, π−π, dipole−induced dipole, and π−induced dipole interactions. These interactions are also causing a preorganization effect between the attacking monomer and the dimer.

These static simulations already provide insights into the governing interactions, but as there is a substantial conformational freedom in the TS region and to obtain further in-depth insights into both the preorganization effect and the intrinsic reaction kinetics, the CROP reaction was further investigated by using enhanced sampling MD simulations.

Overall Reactivity Pattern Using Enhanced Sampling MD Simulations. An accurate description of the free energy

https://dx.doi.org/10.1021/acs.macromol.0c00865
Macromolecules 2020, 53, 3832−3846

profiles is imperative to understand the influence of the degree of unsaturation on the intrinsic reactivity of the 2-oxazoline monomers. To this end, enhanced sampling simulations, namely umbrella sampling simulations, were performed for each system to investigate the effect of the side-chain on the activation barriers and to account for the conformational flexibility of the TS region (*vide supra*). The results are shown in Table 1, and the corresponding energy profiles can be found in section S2.2.2.1 and Figures S12−S15.

Table 1. Intrinsic Helmholtz Free Energies of Activation and Propagation Rate Constants (k_p) for the Model Trimeric Systems under Investigation Obtained via US Simulations[a]

monomer	$\Delta F^{\ddagger}_{fwd}$ (kJ/mol)	$\Delta F^{\ddagger}_{bwd}$ (kJ/mol)	k_p[a] (s^{-1})
n-ButylOx (**a**)	64	105	7.2×10^4
ButenOx (**b**)	63	100	1.0×10^5
ButynOx (**c**)	63	100	9.9×10^4
PentynOx (**d**)	67	116	3.0×10^4

[a]Note that this k_p is not equal to the experimentally measured apparent rate constant (BLYP/TZVP-GTH, 413 K, NVT). Calculated based on the method described by Bailleul et al.[90]

Interestingly, the intrinsic reaction kinetics seem to be barely affected by the degree of unsaturation in the side-chain. Moreover, the impact of the degree of unsaturation as estimated from the propagation rate constants does not agree with the conclusions drawn from the regular MD simulation nor from the static calculations. The effect of unsaturation in the side-chain on the reactant, product, or TS regions is in first instance assessed by calculating the RMSD between different snapshots corresponding to a specific value of the collective variable (see section S2.2.2.1.1). However, no preferred states were observed, and further exploration was needed. Hence, at second instance the one-dimensional free energy profiles were transformed to two-dimensional free energy surfaces in terms of a new set of collective variables that is chosen based on the conclusions from the NCI analysis. Moreover, these variables are expected to show preferred conformations (and hence preferred CV values) within the reactant, product, and/or TS region. To construct two-dimensional free energy profiles, extra information was extracted from the US trajectories in the form of conditional probabilities. More details on this transformation can be found in section S1.3. These profiles not only reveal the broadness of the product, TS, and reactant region (in line with the RMSD results) but also give further insights into preferred reactant and TS regions with respect to this new set of collective variables shown in the 2D free energy profiles (Figure 4, section S2.2.2.1.1, and Figures S18−S22). Herein, as is the case for all shown profiles, the *x*-axis represents the CV defined in Scheme 3 with the reactant region situated from 1 to 5.4 Å (hence on the right side of the profiles), and the product region is from −2.6 to −1 Å (on the left side).

Overall the proposed collective variables do not provide new insights into possible stabilizing effects within the TS region apart from the previously discussed cation−dipole interaction (see section S2.2.2.1.1 and Figure S21). Nonetheless, for the prereactive complex region a clear stabilization occurs when increasing the degree of unsaturation. This indicates that the preorganization effect will not manifest itself by stabilizing the TS but it will by stabilizing the reactant region. Figure 4 nicely illustrated this effect by the occurrence of a more stable prereactive complex region appearing around D3 equal to 4.5 Å for monomers **1a** to **1c** (also section 2.2.2.1, Figure S19 D2, and Figure S21 D5 show this trend). This observation holds for PentynOx (**1d**) as well and is entirely in agreement with the preorganization effect extracted from the NCI-analysis.

From these computational results we conclude that the reaction kinetics will not only be controlled by the intrinsic reactivity of the monomer and propagating cationic chain-end but should be described by a two-step mechanism, similar to the approach of Değirmenci et al., where the apparent rate constant can be split into two contributions: on the one hand, the equilibration constant (K_1) which accounts for the association (k_1) and dissociation (k_{-1}) of the growing polymer chain and the attacking monomer and, on the other hand, the CROP propagation rate constant (k_p) (see Scheme 6).[93,94]

Based on the steady-state approximation, the apparent rate constant for the first-order reaction kinetics is in this case defined as

$$k_{app} = K_1 k_p = \frac{k_1 k_p}{k_{-1} + k_p}$$

To this end the prereactive complexes of the previously discussed most stable TSs (see Figures 2 and 3 **a1**, **b1**, **b2**, **c1**, and **d2**) are calculated statically (see section S2.2.2.2). By combination of the enhanced MD simulations with these static DFT calculations, the role of the observed preorganization effect is clarified. In Figure 5, the free energy profiles for both the equilibration step and the CROP reaction step are displayed schematically. The prereactive complexes of the most stable TSs are highlighted in bold. Note that the free energy differences obtained for the equilibration step of the separate reactants and thus the formation of the prereactive complex are obtained from static calculations while the CROP reaction barriers are obtained from enhanced MD simulations.

On the left, a clear difference exists in the equilibration step with formation of the prereactive complex depending on the degree of unsaturation. The trend reveals that an increasing degree of unsaturation favors the formation of the prereactive complex and thus also favors the reaction kinetics (by its effect on k_{app}), with a decrease in Gibbs free energy of 14 and 27 kJ mol^{-1} for the prereactive complex of the most stable TSs of ButenOx and ButynOx with respect to *n*-ButylOx. This trend is also valid for the other computed prereactive complexes (see Table S6). Furthermore, the side-chain length also affects the formation of the prereactive complex as it is slightly less stable for PentynOx than for ButynOx (−43 and −47 kJ mol^{-1}, respectively). This side-chain length dependence is, however, not seen for all selected TSs which is attributed to the entropy effects which are poorly accounted for in this static approach. Additionally the prereactive complexes were reoptimized by using an implicit solvent model to get a first indication of the influence of the solvent (see section S2.2.2.2 and Table S6, values between brackets), which indeed reveal more stable complexes in the presence of an unsaturated side chain.

As the polymerization experimentally takes place in the presence of acetonitrile, it needs to be verified whether the preorganization effect through cation−π interactions still occurs in the presence of acetonitrile, where also a competitive stabilization with the cationic center could occur through the π bonds of the acetonitrile environment. To assess its effect on the cation−π interactions in the prereactive complex region,

https://dx.doi.org/10.1021/acs.macromol.0c00865
Macromolecules 2020, 53, 3832−3846

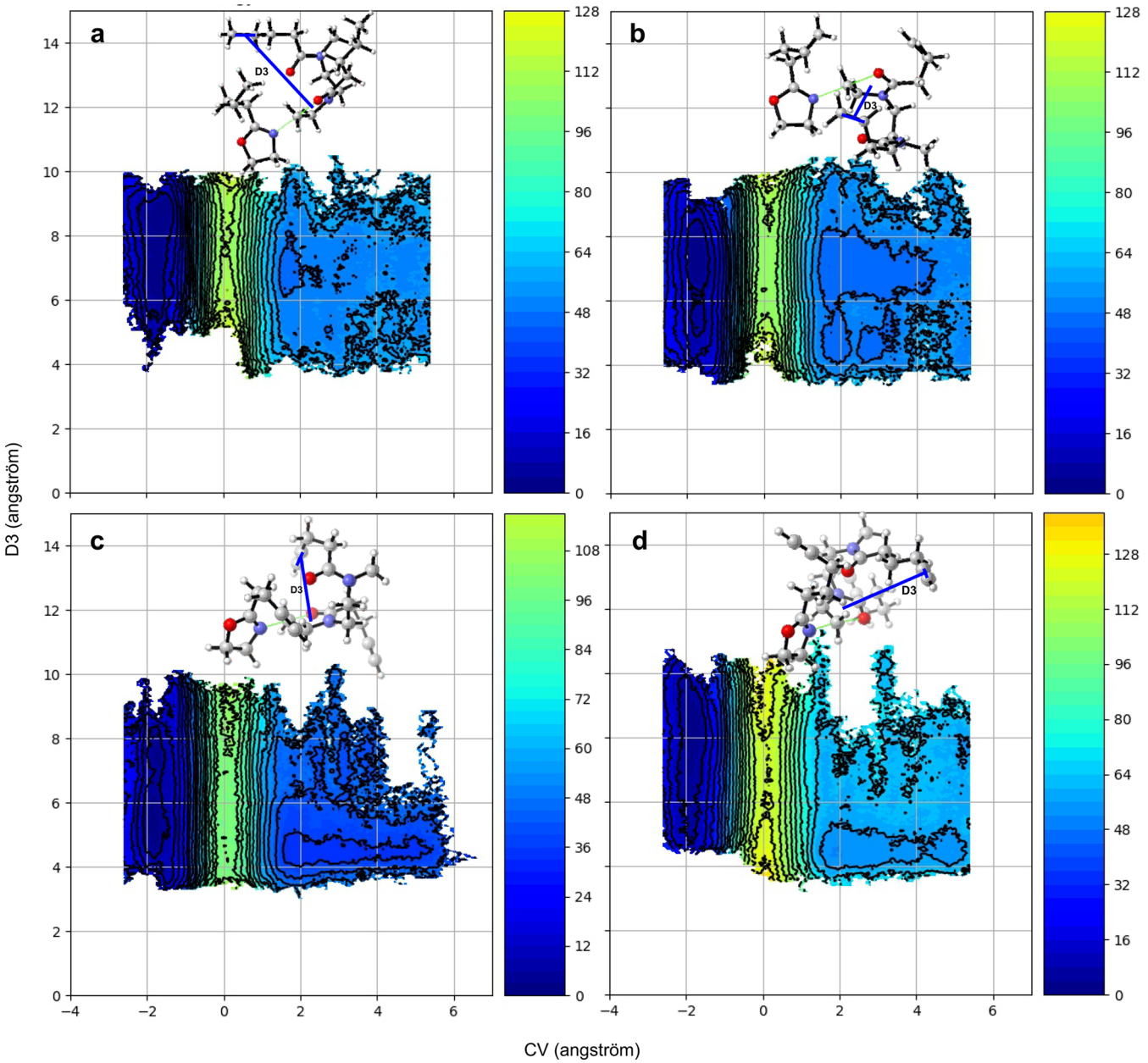

Figure 4. Two-dimensional free energy profiles for ButylOx (**a**), ButenOx (**b**), ButynOx (**c**), and PentynOx (**d**) constructed based on the method described in section S1.3. Color scale is in kJ mol^{-1}. The proposed new collective variable is the distance of the penultimate bond of the terminal side-chain and the cationic center shown in blue in the structures (D3) and represented by the *y*-axis. The *x*-axis is the collective variable describing the reaction, which is sampled in the US simulations. The reactant region is on the right and the product region on the left.

Scheme 6. Reaction Steps Controlling the Kinetics for the CROP of the Investigated 2-Alkyl-2-oxazolines; Monomer M, Polymer P^+, and Prereactive Complex $M{-}P^+$

$$M + P^+ \underset{k_{-1}}{\overset{k_1}{\rightleftharpoons}} M\cdots P^+$$

$$M\cdots P^+ \xrightarrow{k_P} P^+$$

US simulations are performed by using the DFTB method in this specific part of the reaction profile. The ability of DFTB to capture cation−π interactions was first benchmarked by using the pentameric *n*-ButylOx and ButynOx systems (see section S2.2.3.1). The cation−π interactions in the prereactive complex region are again analyzed by constructing two-dimensional free energy profiles based on conditional probabilities. The results are shown in Figure 6 and section S2.2.3.2 and indicate that even in the presence of acetonitrile the cation−π interactions are present in a wide range of the prereactive complex region (see [1] and [2] in Figure 6). This can be seen from the short distances attained by D1, which represents the distance between the attacking monomer π-bond and the cationic center, even at CV values of 6−7.5 Å. In case acetonitrile would destroy the cation−π interactions, these interacting distances would have not been observed. Remarkably, there is no significant barrier observed between the prereactive complex region and the region in which no interactions occur between the monomer and the dimer (7.5−11 Å); this potentially indicates that the CV of our choice is not a proper variable to account for this preorganization effect

https://dx.doi.org/10.1021/acs.macromol.0c00865
Macromolecules 2020, 53, 3832−3846

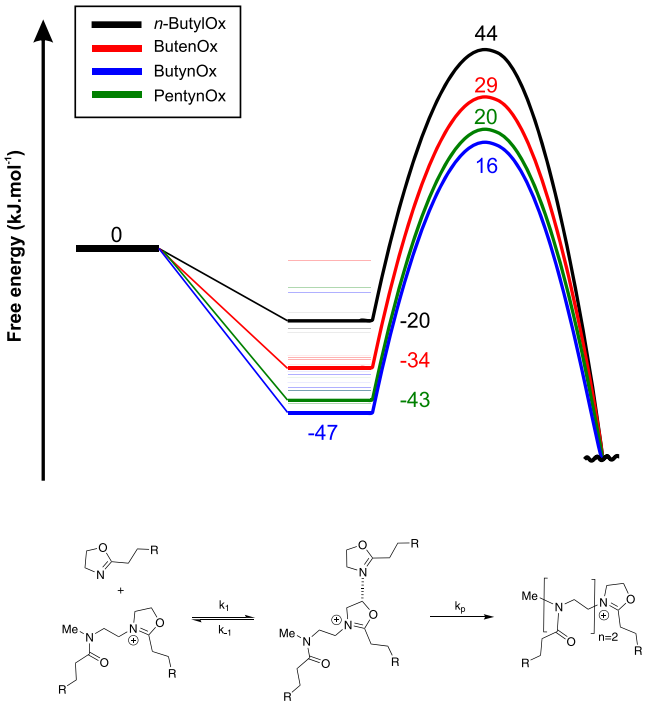

Figure 5. Combined free energy profile for the equilibration step and the actual polymerization step of the CROP reaction for the different 2-oxazolines under investigation. The equilibration step is obtained by static calculations for multiple prereactive complexes, of which an overview is found in section S2.2.2.2, the polymerization step by enhanced MD simulations. *n*-ButylOx is shown in black, ButenOx in red, ButynOx in blue, and PentynOx in green.

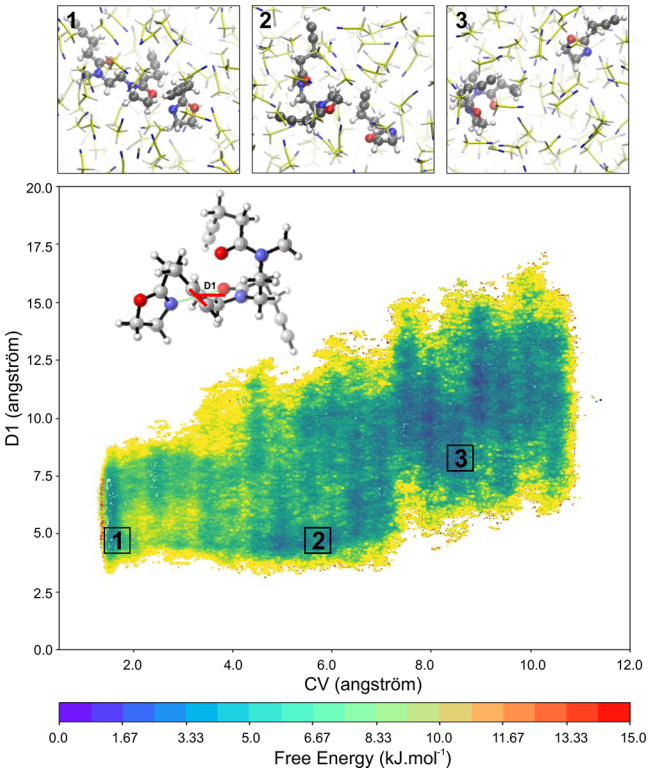

Figure 6. Two-dimensional free energy profile for ButynOx in the presence of acetonitrile constructed based on the method described in section S1.3. Color scale is in kJ mol^{-1}. The proposed new collective variable is the distance of the penultimate bond of the attacking monomer side-chain toward the cationic center shown in red in the structure (D1) and represented by the *y*-axis. The *x*-axis is the collective variable describing the reaction, which is used to sample the prereactive complex region through US simulations. The reactant region is shown spanning from 1.0 to 10.5 Å. Snapshots on the top of the figure indicate the presence of cation−π interaction in an explicit solvent environment.

as it is unable to distinguish between an interacting state and a noninteracting state within an explicit solvent environment. More work is necessary to study how proper collective variables may be chosen in the presence of solvents. This is however beyond the scope of this study.

Hence, overall these results predict a difference in rate constants between the different systems based on the association behavior of the monomer and the growing polymer involved in the CROP reaction of 2-alkyl-2-oxazolines. It is thus anticipated that the apparent propagation rate constants for the polymerization kinetics for the different systems will show the following trend: *n*-ButylOx < ButenOx < ButynOx ≥ PentynOx. This trend is equal to the one predicted during the thorough static analysis of the transition state region of the different 2-oxazolines. Importantly, this more advanced analysis revealed that the difference in reactivity due to the cation−π interactions affects the association behavior of the monomer with the growing polymer chain rather than the intrinsic barrier heights of the CROP propagation reaction. Furthermore, it was shown that the preorganization effect based on cation−π, π−π, and π−induced dipole interactions is responsible for this difference in association behavior even in the presence of acetonitrile.

Experimental Results. To assess how the computationally established cation−π interactions (*vide supra*) translate in an acceleration of the CROP of 2-oxazoline monomers with unsaturated side-chains, the monomers **1a−d** were synthesized and their polymerization kinetics determined, as will be discussed in the following. Full experimental details, including the single crystal X-ray structure of monomer **1c**, are included in section S3.

Polymerization Kinetics. The polymerization kinetics of the monomers were investigated under the same, previously optimized, conditions, namely in acetonitrile with 4 M monomer concentration and methyl tosylate as initiator (monomer to initiator ratio of 100) at 140 °C under microwave irradiation. For all the monomers, the first-order kinetic plots of monomer consumption with respect to the reaction time revealed a linear relationship (Figure 7), thus demonstrating a constant amount of propagating species indicative of the absence of termination as well as fast initiation. Furthermore, the number-average molecular weight (M_n) increased linearly with conversion, while the dispersity ($Đ$) remained below 1.30 (see section S3.3 as well as Figures S27 and S28), demonstrating that the polymerizations proceeded in a living/controlled manner. The first-order kinetic plot (Figure 7) clearly revealed that the polymerization rate constant changes upon variation of the substituent in the 2-position. The unsaturated monomers polymerize significantly faster than *n*-ButylOx (k_p = (94 ± 6) × 10^{-3} L mol^{-1} s^{-1}), ranging from a factor of 2 for ButenOx (k_p = (200 ± 10) × 10^{-3} L mol^{-1} s^{-1}) to an increase in rate by a factor of 4−5 for PentynOx (k_p = (416 ± 3) × 10^{-3} L mol^{-1} s^{-1}) and ButynOx (k_p = (496 ± 11) × 10^{-3} L mol^{-1} s^{-1}). Within the field of polymerization reactions, such 4-fold rate enhancements are regarded as significant.[12,93,95−101] Nonetheless, such rate accelerations correspond to relatively minor differences in reaction barriers of only a few kJ/mol, which is a challenge for theoretical methods to achieve. Nonetheless, as we systematically found differences in the intermolecular interactions with a broad range of methods and in the presence of solvent, there is solid evidence for the theoretically established acceleration of the CROP by cation−π interactions of unsaturated bonds in the 2-oxazoline monomer side-chains.

https://dx.doi.org/10.1021/acs.macromol.0c00865
Macromolecules 2020, 53, 3832−3846

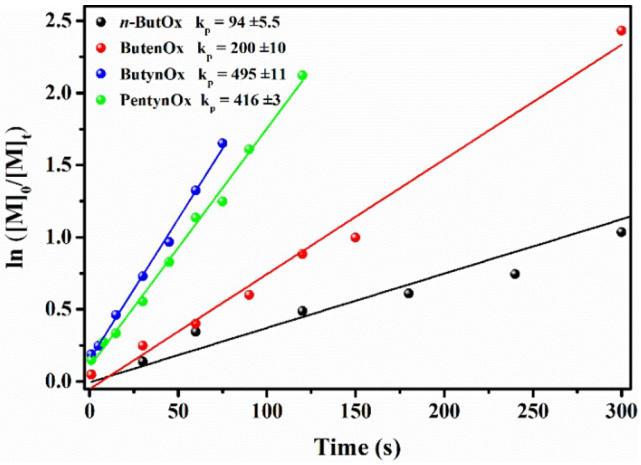

Figure 7. First-order kinetic plot for the cationic ring-opening polymerization of *n*-ButOx, ButenOx, ButynOx, and PentynOx. Polymerizations were performed at 140 °C in acetonitrile with 4 M monomer (M) concentration, methyl tosylate (I) as initiator, and a [M]:[I] ratio of 100. The polymerization rate constants (k_p's) are given in 10^{-3} L mol^{-1} s^{-1}.

CONCLUSIONS

In this work, we have established proof for the presence of cation−π interactions in ButenOx, ButynOx, and PentynOx by first-principles MD simulations, as these were not present in the reference system (*n*-ButylOx). Additionally, an effect of the degree of unsaturation is theoretically confirmed, and an entropic penalty for the longer side-chain is observed. To explore to what extent the intrinsic kinetics are affected by the side-chain, complementary calculations have been performed on the second propagation step of the CROP in combination with a thorough analysis of the governing noncovalent interactions. First a static approach revealed that complex interaction patterns are governing a very broad transition state region, and it was concluded that an interplay occurs between cation−π, π−π, π−induced dipole, and cation−dipole interactions. These interactions were also shown to enable a preorganization effect between the attacking monomer and the growing polymer chain-end. Furthermore, a larger entropic dependence of the PentynOx system, suggested by the regular MD simulations, was confirmed. Second, because of the substantial conformational freedom, enhanced sampling MD simulations were performed to accurately describe the effect of the side-chain on the intrinsic barrier heights. Limited effects were observed, and hereto the width of reactant, product, and transition state regions was assessed by the construction of two-dimensional free energy surfaces through conditional probabilities, extracted from the enhanced sampling simulations. These revealed that the previously observed preorganization effect enables stabilization of preferentially the prereactive complex region through the presence of cation−π interactions among others. Combining the conclusion of the static and enhanced sampling approach led to the proposal of a two-step mechanism involving the equilibration process with formation of the prereactive complex next to the actual CROP step. By use of a static approach, the equilibration step of the reactants toward the prereactive complex is shown to be the rate-determining step, as a clear difference is observed depending on the degree of unsaturation of the side-chain. Based on the computational conclusions, the following trend in reaction kinetics was anticipated, which was then confirmed by experiments that revealed the following order in the apparent propagation rate constants: *n*-ButylOx < ButenOx < ButynOx ≥ PentynOx. The insights obtained in this study are potentially of great importance to different monomers which polymerize through a cationic, or even anionic, polymerization mechanism. Our study clearly shows how the polymerization kinetics can be altered through preorganization effects induced by interactions between the active center of the growing polymer and neighboring group effects. Irrespective of the specific results for this polymerization system, the modeling strategy yields valuable information about how to investigate polymerization kinetics and the way it is affected by noncovalent, stabilizing interactions and by the presence of solvent interactions. With regard to the modeling of polymerization reactions, we have shown that investigating trimeric systems suffices to investigate both intrinsic reactivity and side-chain flexibility, in line with previous study by Izgorodina et al.[102] Furthermore, in case a stabilizing interaction occurs within the transition states, e.g., cation−π or π−π interactions, these potentially have no net effect on the intrinsic reactivity because similar stabilization effects occur in the prereactive complex region. To finalize, preorganization effects established through the aforementioned interactions can induce significant rate-enhancing effects by guiding the growth of the polymer more efficiently. Such effects might be of great importance in copolymerization reactions to control monomer distributions within the resulting polymers.

ASSOCIATED CONTENT

Supporting Information

The Supporting Information is available free of charge at https://pubs.acs.org/doi/10.1021/acs.macromol.0c00865.

Figures S1−S28, Schemes S1−S3, and Tables S1−S6 (PDF)

Crystallographic data (CIF)

AUTHOR INFORMATION

Corresponding Authors

Veronique Van Speybroeck − *Center for Molecular Modeling, Ghent University, 9052 Zwijnaarde, Belgium;* orcid.org/0000-0003-2206-178X; Email: veronique.vanspeybroeck@ugent.be

Richard Hoogenboom − *Supramolecular Chemistry Group, Centre of Macromolecular Chemistry (CMaC), Department of Organic and Macromolecular Chemistry, Ghent University, 9000 Gent, Belgium;* orcid.org/0000-0001-7398-2058; Email: Richard.hoogenboom@ugent.be

Authors

Elias Van Den Broeck − *Center for Molecular Modeling, Ghent University, 9052 Zwijnaarde, Belgium;* orcid.org/0000-0002-9609-4333

Bart Verbraeken − *Supramolecular Chemistry Group, Centre of Macromolecular Chemistry (CMaC), Department of Organic and Macromolecular Chemistry, Ghent University, 9000 Gent, Belgium*

Karen Dedecker − *Center for Molecular Modeling, Ghent University, 9052 Zwijnaarde, Belgium*

Pieter Cnudde − *Center for Molecular Modeling, Ghent University, 9052 Zwijnaarde, Belgium;* orcid.org/0000-0002-6735-0078

https://dx.doi.org/10.1021/acs.macromol.0c00865
Macromolecules 2020, 53, 3832−3846

Louis Vanduyfhuys − *Center for Molecular Modeling, Ghent University, 9052 Zwijnaarde, Belgium*

Toon Verstraelen − *Center for Molecular Modeling, Ghent University, 9052 Zwijnaarde, Belgium;* orcid.org/0000-0001-9288-5608

Kristof Van Hecke − *XStruct, Department of Chemistry, Ghent University, B-9000 Ghent, Belgium;* orcid.org/0000-0002-2455-8856

Valentin Victor Jerca − *Supramolecular Chemistry Group, Centre of Macromolecular Chemistry (CMaC), Department of Organic and Macromolecular Chemistry, Ghent University, 9000 Gent, Belgium; Centre for Organic Chemistry "Costin D. Nenitzescu", Romanian Academy, Bucharest 060023, Romania;* orcid.org/0000-0001-6997-4979

Saron Catak − *Center for Molecular Modeling, Ghent University, 9052 Zwijnaarde, Belgium; Department of Chemistry, Bogazici University, 34342 Istanbul, Turkey;* orcid.org/0000-0002-4396-8375

Complete contact information is available at: https://pubs.acs.org/10.1021/acs.macromol.0c00865

Author Contributions

E.V.D.B. and B.V. contributed equally to this work.

Notes

The authors declare no competing financial interest.

■ ACKNOWLEDGMENTS

The computational resources and services used were provided by Ghent University (Stevin Supercomputer Infrastructure), the VSC (Flemish Supercomputer Center), funded by the Research Foundation - Flanders (FWO). Further this work is supported by the Research Board of the Ghent University (BOF). K.V.H. thanks the Special Research Fund (BOF) − UGent (project 01N03217) for funding. V.V.S., P.C., and K.D. acknowledge funding from the European Union's Horizon 2020 research and innovation program (consolidator ERC grant agreement no. 647755 - DYNPOR (2015-2020)). The Fund for Scientific Research Flanders and the Research Board of the Ghent University (BOF) is acknowledged for funding.

■ REFERENCES

(1) Bassiri, T. G.; Levy, A.; Litt, M. Polymerization of Cyclic Imino Ethers. I. Oxazolines. *J. Polym. Sci., Part B: Polym. Lett.* **1967**, *5* (9), 871−879.

(2) Seeliger, W.; Aufderhaar, E.; Diepers, W.; Feinauer, R.; Nehring, R.; Thier, W.; Hellmann, H. Recent Syntheses and Reactions of Cyclic Imidic Esters. *Angew. Chem., Int. Ed. Engl.* **1966**, *5* (10), 875−888.

(3) Tomalia, D. A.; Sheetz, D. P. Homopolymerization of 2-Alkyl- and 2-Aryl-2-Oxazolines. *J. Polym. Sci., Part A-1: Polym. Chem.* **1966**, *4* (9), 2253−2265.

(4) Kagiya, T.; Narisawa, S.; Maeda, T.; Fukui, K. Ring-Opening Polymerization of 2-Substituted 2-Oxazolines. *J. Polym. Sci., Part B: Polym. Lett.* **1966**, *4* (7), 441−445.

(5) Zalipsky, S.; Hansen, C. B.; Oaks, J. M.; Allen, T. M. Evaluation of Blood Clearance Rates and Biodistribution of Poly(2-Oxazoline)-Grafted Liposomes§. *J. Pharm. Sci.* **1996**, *85* (2), 133−137.

(6) Mero, A.; Pasut, G.; Via, L. D.; Fijten, M. W. M.; Schubert, U. S.; Hoogenboom, R.; Veronese, F. M. Synthesis and Characterization of Poly(2-Ethyl 2-Oxazoline)-Conjugates with Proteins and Drugs: Suitable Alternatives to PEG-Conjugates? *J. Controlled Release* **2008**, *125* (2), 87−95.

(7) Luxenhofer, R.; Han, Y.; Schulz, A.; Tong, J.; He, Z.; Kabanov, A. V.; Jordan, R. Poly(2-Oxazoline)s as Polymer Therapeutics. *Macromol. Rapid Commun.* **2012**, *33* (19), 1613−1631.

(8) Hoogenboom, R. Poly(2-Oxazoline)s: A Polymer Class with Numerous Potential Applications. *Angew. Chem., Int. Ed.* **2009**, *48* (43), 7978−7994.

(9) Monnery, B. D.; Jerca, V. V.; Sedlacek, O.; Verbraeken, B.; Cavill, R.; Hoogenboom, R. Defined High Molar Mass Poly(2-Oxazoline)S. *Angew. Chem., Int. Ed.* **2018**, *57* (47), 15400−15404.

(10) Goossens, H.; Catak, S.; Glassner, M.; de la Rosa, V. R.; Monnery, B. D.; De Proft, F.; Van Speybroeck, V.; Hoogenboom, R. Cationic Ring-Opening Polymerization of 2-Propyl-2-Oxazolines: Understanding Structural Effects on Polymerization Behavior Based on Molecular Modeling. *ACS Macro Lett.* **2013**, *2* (8), 651−654.

(11) Bouten, P. J. M.; Hertsen, D.; Vergaelen, M.; Monnery, B. D.; Catak, S.; van Hest, J. C. M.; Van Speybroeck, V.; Hoogenboom, R. Synthesis of Poly(2-Oxazoline)s with Side Chain Methyl Ester Functionalities: Detailed Understanding of Living Copolymerization Behavior of Methyl Ester Containing Monomers with 2-Alkyl-2-Oxazolines. *J. Polym. Sci., Part A: Polym. Chem.* **2015**, *53* (22), 2649−2661.

(12) Bouten, P. J. M.; Hertsen, D.; Vergaelen, M.; Monnery, B. D.; Boerman, M. A.; Goossens, H.; Catak, S.; van Hest, J. C. M.; Van Speybroeck, V.; Hoogenboom, R. Accelerated Living Cationic Ring-Opening Polymerization of a Methyl Ester Functionalized 2-Oxazoline Monomer. *Polym. Chem.* **2015**, *6*, 514−518.

(13) Luef, K. P.; Hoogenboom, R.; Schubert, U. S.; Wiesbrock, F. Microwave-Assisted Cationic Ring-Opening Polymerization of 2-Oxazolines. *Adv. Polym. Sci.* **2015**, *274*, 183−208.

(14) Hoogenboom, R.; Fijten, M. W. M.; Thijs, H. M. L.; van Lankvelt, B. M.; Schubert, U. S. Microwave-Assisted Synthesis and Properties of a Series of Poly(2-Alkyl-2-Oxazoline)S. *Des. Monomers Polym.* **2005**, *8* (6), 659−671.

(15) Lobert, M.; Köhn, U.; Hoogenboom, R.; Schubert, U. S. Synthesis and Microwave Assisted Polymerization of Fluorinated 2-Phenyl-2-Oxazolines: The Fastest 2-Oxazoline Monomer to Date. *Chem. Commun.* **2008**, *0* (12), 1458.

(16) Bloksma, M. M.; Schubert, U. S.; Hoogenboom, R. Poly(Cyclic Imino Ether)s Beyond 2-Substituted-2-Oxazolines. *Macromol. Rapid Commun.* **2011**, *32* (18), 1419−1441.

(17) Hallett, A. J.; O'Brien, T. M.; Carter, E.; Kariuki, B. M.; Murphy, D. M.; Ward, B. D. Copper(II) Complexes of Pyridine-Oxazoline (Pyox) Ligands: Coordination Chemistry, Ligand Stability, and Catalysis. *Inorg. Chim. Acta* **2016**, *441*, 86−94.

(18) Kim, S.-G.; Kim, K.-H.; Jung, J.; Shin, S. K.; Ahn, K. H. Unprecedented Chiral Molecular Recognition in a C3-Symmetric Environment. *J. Am. Chem. Soc.* **2002**, *124* (4), 591−596.

(19) Fritschi, H.; Leutenegger, U.; Pfaltz, A. Chiral Copper-Semicorrin Complexes as Enantioselective Catalysts for the Cyclopropanation of Olefins by Diazo Compounds. *Angew. Chem., Int. Ed. Engl.* **1986**, *25* (11), 1005−1006.

(20) Bellemin-Laponnaz, S.; Gade, L. H. A Modular Approach to C1 and C3 Chiral N-Tripodal Ligands for Asymmetric Catalysis. *Angew. Chem., Int. Ed.* **2002**, *41* (18), 3473−3475.

(21) Knop, K.; Hoogenboom, R.; Fischer, D.; Schubert, U. S. Poly(Ethylene Glycol) in Drug Delivery: Pros and Cons as Well as Potential Alternatives. *Angew. Chem., Int. Ed.* **2010**, *49* (36), 6288−6308.

(22) Luef, K. P.; Petit, C.; Ottersböck, B.; Oreski, G.; Ehrenfeld, F.; Grassl, B.; Reynaud, S.; Wiesbrock, F. UV-Mediated Thiol-Ene Click Reactions for the Synthesis of Drug-Loadable and Degradable Gels Based on Copoly(2-Oxazoline)S. *Eur. Polym. J.* **2017**, *88*, 701−712.

(23) Gress, A.; Völkel, A.; Schlaad, H. Thio-Click Modification of Poly[2-(3-Butenyl)-2-Oxazoline]. *Macromolecules* **2007**, *40* (22), 7928−7933.

(24) Hoogenboom, R.; Schlaad, H. Bioinspired Poly(2-Oxazoline)S. *Polymers (Basel, Switz.)* **2011**, *3* (4), 467−488.

(25) Kelly, A. M.; Hecke, A.; Wirnsberger, B.; Wiesbrock, F. Synthesis of Poly(2-Oxazoline)-Based Hydrogels with Tailor-Made

Swelling Degrees Capable of Stimuli-Triggered Compound Release. *Macromol. Rapid Commun.* **2011**, *32* (22), 1815−1819.
(26) Bouten, P.; Lava, K.; van Hest, J.; Hoogenboom, R. Thermal Properties of Methyl Ester-Containing Poly(2-Oxazoline)S. *Polymers (Basel, Switz.)* **2015**, *7* (12), 1998−2008.
(27) Katagiri, K.; Takasu, A.; Higuchi, M. Synthesis of Glycopolymer Containing Cell-Penetrating Peptides as Inducers of Recombinant Protein Expression under the Control of Lactose Operator/Repressor Systems. *Biomacromolecules* **2016**, *17* (5), 1902−1908.
(28) Manzenrieder, F.; Luxenhofer, R.; Retzlaff, M.; Jordan, R.; Finn, M. G. Stabilization of Virus-like Particles with Poly(2-Oxazoline)S. *Angew. Chem., Int. Ed.* **2011**, *50* (11), 2601−2605.
(29) Bissadi, G.; Weberskirch, R. Efficient Synthesis of Polyoxazoline-Silica Hybrid Nanoparticles by Using the "Grafting-onto" Approach. *Polym. Chem.* **2016**, *7* (6), 1271−1280.
(30) Tauhardt, L.; Kempe, K.; Gottschaldt, M.; Schubert, U. S. Poly(2-Oxazoline) Functionalized Surfaces: From Modification to Application. *Chem. Soc. Rev.* **2013**, *42* (42), 7998−8011.
(31) Engelhardt, N.; Ernst, A.; Kampmann, A.-L.; Weberskirch, R. Synthesis and Characterization of Surface Functional Polymer Nanoparticles by a Bottom-Up Approach from Tailor-Made Amphiphilic Block Copolymers. *Macromol. Chem. Phys.* **2013**, *214* (24), 2783−2791.
(32) Trumbo, D. L. Epoxidized Poly(Decenyloxazoline) in Thermoset Coatings. *J. Coatings Technol. Res.* **2006**, *3* (1), 87−88.
(33) Hayashi, T.; Takasu, A. Design of Electrophoretic and Biocompatible Poly(2-Oxazoline)s Initiated by Perfluoroalkanesulfoneimides and Electrophoretic Deposition with Bioactive Glass. *Biomacromolecules* **2015**, *16* (4), 1259−1266.
(34) Rother, M.; Nussbaumer, M. G.; Renggli, K.; Bruns, N. Protein Cages and Synthetic Polymers: A Fruitful Symbiosis for Drug Delivery Applications, Bionanotechnology and Materials Science. *Chem. Soc. Rev.* **2016**, *45* (22), 6213−6249.
(35) Ying, W. B.; Kim, S.; Lee, M. W.; Go, N. Y.; Jung, H.; Ryu, S. G.; Lee, B.; Lee, K. J. Toward a Detoxification Fabric against Nerve Gas Agents: Guanidine-Functionalized Poly[2-(3-Butenyl)-2-Oxazoline]/Nylon-6,6 Nanofibers. *RSC Adv.* **2017**, *7* (25), 15246−15254.
(36) ten Brummelhuis, N.; Schlaad, H. Stimuli-Responsive Star Polymers through Thiol-Yne Core Functionalization/Crosslinking of Block Copolymer Micelles. *Polym. Chem.* **2011**, *2* (5), 1180.
(37) Diehl, C.; Schlaad, H. Thermo-Responsive Polyoxazolines with Widely Tuneable LCST. *Macromol. Biosci.* **2009**, *9* (2), 157−161.
(38) Hartlieb, M.; Kempe, K.; Schubert, U. S. Covalently Cross-Linked Poly(2-Oxazoline) Materials for Biomedical Applications - from Hydrogels to Self-Assembled and Templated Structures. *J. Mater. Chem. B* **2015**, *3* (4), 526−538.
(39) Fimberger, M.; Behrendt, A.; Jakopic, G.; Stelzer, F.; Kumbaraci, V.; Wiesbrock, F. Modification Pathways for Copoly(2-Oxazoline)s Enabling Their Application as Antireflective Coatings in Photolithography. *Macromol. Rapid Commun.* **2016**, *37* (3), 233−238.
(40) Schmitz, M.; Kuhlmann, M.; Reimann, O.; Hackenberger, C. P. R.; Groll, J. Side-Chain Cysteine-Functionalized Poly(2-Oxazoline)s for Multiple Peptide Conjugation by Native Chemical Ligation. *Biomacromolecules* **2015**, *16* (4), 1088−1094.
(41) Dargaville, T. R.; Lava, K.; Verbraeken, B.; Hoogenboom, R. Unexpected Switching of the Photogelation Chemistry When Cross-Linking Poly(2-Oxazoline) Copolymers. *Macromolecules* **2016**, *49* (13), 4774−4783.
(42) Lee, L.-C.; Lu, J.; Weck, M.; Jones, C. W. Acid-Base Bifunctional Shell Cross-Linked Micelle Nanoreactor for One-Pot Tandem Reaction. *ACS Catal.* **2016**, *6* (2), 784−787.
(43) Dargaville, T. R.; Park, J. R.; Hoogenboom, R. Poly(2-Oxazoline) Hydrogels: State-of-the-Art and Emerging Applications. *Macromol. Biosci.* **2018**, *18* (6), 1800070.
(44) Park, J.-S.; Kataoka, K. Comprehensive and Accurate Control of Thermosensitivity of Poly(2-Alkyl-2-Oxazoline)s via Well-Defined Gradient or Random Copolymerization. *Macromolecules* **2007**, *40* (10), 3599−3609.
(45) Kobayashi, S.; Tokuzawa, T.; Saegusa, T. Cationic Ring-Opening Isomerization Polymerization of 2-[p-(Substituted)Phenyl]-2-Oxazolines. Effects of the Substituent on the Reactivities. *Macromolecules* **1982**, *15* (3), 707−710.
(46) Grimme, S.; Antony, J.; Ehrlich, S.; Krieg, H. A Consistent and Accurate *Ab Initio* Parametrization of Density Functional Dispersion Correction (DFT-D) for the 94 Elements H-Pu. *J. Chem. Phys.* **2010**, *132* (15), 154104.
(47) Piens, N.; Goossens, H.; Hertsen, D.; Deketelaere, S.; Crul, L.; Demeurisse, L.; De Moor, J.; Van den Broeck, E.; Mollet, K.; Van Hecke, K.; et al. Reactivity of 3-Oxo-β-Lactams with Respect to Primary Amines-An Experimental and Computational Approach. *Chem. - Eur. J.* **2017**, *23* (71), 18002−18009.
(48) Burns, L. A.; Mayagoitia, Á. V.; Sumpter, B. G.; Sherrill, C. D. Density-Functional Approaches to Noncovalent Interactions: A Comparison of Dispersion Corrections (DFT-D), Exchange-Hole Dipole Moment (XDM) Theory, and Specialized Functionals. *J. Chem. Phys.* **2011**, *134* (8), 084107.
(49) Peng, Q.; Duarte, F.; Paton, R. S. Computing Organic Stereoselectivity - from Concepts to Quantitative Calculations and Predictions. *Chem. Soc. Rev.* **2016**, *47* (51), 6081−6408.
(50) Goerigk, L.; Grimme, S. A Thorough Benchmark of Density Functional Methods for General Main Group Thermochemistry, Kinetics, and Noncovalent Interactions. *Phys. Chem. Chem. Phys.* **2011**, *13* (14), 6670−6688.
(51) Dykstra, C. E. *Theory and Applications of Computational Chemistry: The First Forty Years*; Elsevier: 2005.
(52) Fukui, K. The Path of Chemical Reactions - the IRC Approach. *Acc. Chem. Res.* **1981**, *14* (12), 363−368.
(53) Hratchian, H. P.; Schlegel, H. B. Accurate Reaction Paths Using a Hessian Based Predictor-Corrector Integrator. *J. Chem. Phys.* **2004**, *120* (21), 9918−9924.
(54) Tomasi, J.; Mennucci, B.; Cammi, R. Quantum Mechanical Continuum Solvation Models. *Chem. Rev.* **2005**, *105*, 2999−3094.
(55) Frisch, M. J.; Trucks, G. W.; Schlegel, H. B.; Scuseria, G. E.; Robb, M. A.; Cheeseman, J. R.; Scalmani, G.; Barone, V.; Petersson, G. A.; Nakatsuji, H.; Li, X.; Caricato, M.; Marenich, A. V.; Bloino, J.; Janesko, B. G.; Gomperts, R.; Mennucci, B.; Hratch, J. B. *Gaussian 16*, Revision A.03; Gaussian Inc.: Wallingford, CT, 2016.
(56) Zheng, S.; Pfaendtner, J. Enhanced Sampling of Chemical and Biochemical Reactions with Metadynamics. *Mol. Simul.* **2015**, *41* (1−3), 55−72.
(57) VandeVondele, J.; Krack, M.; Mohamed, F.; Parrinello, M.; Chassaing, T.; Hutter, J. Quickstep: Fast and Accurate Density Functional Calculations Using a Mixed Gaussian and Plane Waves Approach. *Comput. Phys. Commun.* **2005**, *167* (2), 103−128.
(58) Grimme, S. Supramolecular Binding Thermodynamics by Dispersion-Corrected Density Functional Theory. *Chem. - Eur. J.* **2012**, *18* (32), 9955−9964.
(59) Hutter, J.; Iannuzzi, M.; Schiffmann, F.; VandeVondele, J. Cp2k: Atomistic Simulations of Condensed Matter Systems. *Wiley Interdiscip. Rev. Comput. Mol. Sci.* **2014**, *4* (1), 15−25.
(60) Goedecker, S.; Teter, M.; Hutter, J. Separable Dual-Space Gaussian Pseudopotentials. *Phys. Rev. B: Condens. Matter Mater. Phys.* **1996**, *54* (3), 1703−1710.
(61) Mardirossian, N.; Head-Gordon, M. Thirty Years of Density Functional Theory in Computational Chemistry: An Overview and Extensive Assessment of 200 Density Functionals. *Mol. Phys.* **2017**, *115*, 2315−2372.
(62) Lippert, G.; Hutter, J.; Parrinello, M. A Hybrid Gaussian and Plane Wave Density Functional Scheme. *Mol. Phys.* **1997**, *92* (3), 477−488.
(63) Lippert, G.; Hutter, J.; Parrinello, M. The Gaussian and Augmented-Plane-Wave Density Functional Method for Ab Initio Molecular Dynamics Simulations. *Theor. Chem. Acc.* **1999**, *103* (2), 124−140.
(64) Martyna, G. J.; Klein, M. L.; Tuckerman, M. Nosé-Hoover Chains: The Canonical Ensemble via Continuous Dynamics. *J. Chem. Phys.* **1992**, *97* (4), 2635−2643.

https://dx.doi.org/10.1021/acs.macromol.0c00865
Macromolecules 2020, 53, 3832−3846

(65) Nosé, S. A Molecular Dynamics Method for Simulations in the Canonical Ensemble. *Mol. Phys.* **1984**, *52* (2), 255−268.
(66) Emenike, B. U.; Bey, S. N.; Spinelle, R. A.; Jones, J. T.; Yoo, B.; Zeller, M. Cationic CH···π Interactions as a Function of Solvation. *Phys. Chem. Chem. Phys.* **2016**, *18* (45), 30940−30945.
(67) Emenike, B. U.; Bey, S. N.; Bigelow, B. C.; Chakravartula, S. V. S. Quantitative Model for Rationalizing Solvent Effect in Noncovalent CH-Aryl Interactions. *Chem. Sci.* **2016**, *7* (2), 1401−1407.
(68) Gallivan, J. P.; Dougherty, D. A. A Computational Study of Cation-π Interactions vs Salt Bridges in Aqueous Media: Implications for Protein Engineering. *J. Am. Chem. Soc.* **2000**, *122* (5), 870−874.
(69) Yamada, S.; Yamamoto, N.; Takamori, E. A Molecular Seesaw Balance: Evaluation of Solvent and Counteranion Effects on Pyridinium-π Interactions. *Org. Lett.* **2015**, *17* (19), 4862−4865.
(70) Nagy, E.; St. Germain, E.; Cosme, P.; Maity, P.; Terentis, A. C.; Lepore, S. D. Ammonium Catalyzed Cyclitive Additions: Evidence for a Cation-π Interaction with Alkynes. *Chem. Commun.* **2016**, *52* (11), 2311−2313.
(71) Li, P.; Vik, E. C.; Maier, J. M.; Karki, I.; Strickland, S. M. S.; Umana, J. M.; Smith, M. D.; Pellechia, P. J.; Shimizu, K. D. Electrostatically Driven CO-π Aromatic Interactions. *J. Am. Chem. Soc.* **2019**, *141* (32), 12513−12517.
(72) Zhechkov, L.; Heine, T.; Patchkovskii, S.; Seifert, G.; Duarte, H. A. An Efficient a Posteriori Treatment for Dispersion Interaction in Density-Functional-Based Tight Binding. *J. Chem. Theory Comput.* **2005**, *1* (5), 841−847.
(73) Seifert, G.; Porezag, D.; Frauenheim, T. Calculations of Molecules, Clusters, and Solids with a Simplified LCAO-DFT-LDA Scheme. *Int. J. Quantum Chem.* **1996**, *58* (2), 185−192.
(74) Porezag, D.; Frauenheim, T.; Köhler, T.; Seifert, G.; Kaschner, R. Construction of Tight-Binding-like Potentials on the Basis of Density-Functional Theory: Application to Carbon. *Phys. Rev. B: Condens. Matter Mater. Phys.* **1995**, *51* (19), 12947−12957.
(75) Elstner, M.; Porezag, D.; Jungnickel, G.; Elsner, J.; Haugk, M.; Frauenheim, T.; Suhai, S.; Seifert, G. Self-Consistent-Charge Density-Functional Tight-Binding Method for Simulations of Complex Materials Properties. *Phys. Rev. B: Condens. Matter Mater. Phys.* **1998**, *58* (11), 7260−7268.
(76) Elstner, M.; Seifert, G. Density Functional Tight Binding. *Philos. Trans. R. Soc., A* **2014**, *372*, 20120483.
(77) Davis, M. R.; Dougherty, D. A. Cation-π Interactions: Computational Analyses of the Aromatic Box Motif and the Fluorination Strategy for Experimental Evaluation. *Phys. Chem. Chem. Phys.* **2015**, *17* (43), 29262−29270.
(78) Marshall, M. S.; Steele, R. P.; Thanthiriwatte, K. S.; Sherrill, C. D. Potential Energy Curves for Cation-π Interactions: Off-Axis Configurations Are Also Attractive. *J. Phys. Chem. A* **2009**, *113* (48), 13628−13632.
(79) Giorgino, T. PLUMED-GUI: An Environment for the Interactive Development of Molecular Dynamics Analysis and Biasing Scripts. *Comput. Phys. Commun.* **2014**, *185* (3), 1109−1114.
(80) Humphrey, W.; Dalke, A.; Schulten, K. VMD: Visual Molecular Dynamics. *J. Mol. Graphics* **1996**, *14* (1), 33−38.
(81) Van Erp, T. S.; Moroni, D.; Bolhuis, P. G. A Novel Path Sampling Method for the Calculation of Rate Constants. *J. Chem. Phys.* **2003**, *118* (17), 7762−7774.
(82) Noble, B. B.; Coote, M. L. First Principles Modelling of Free-Radical Polymerisation Kinetics. *Int. Rev. Phys. Chem.* **2013**, *32*, 467−513.
(83) Torrie, G. M.; Valleau, J. P. Nonphysical Sampling Distributions in Monte Carlo Free-Energy Estimation: Umbrella Sampling. *J. Comput. Phys.* **1977**, *23* (2), 187−199.
(84) Torrie, G. M.; Valleau, J. P. Monte Carlo Free Energy Estimates Using Non-Boltzmann Sampling: Application to the Sub-Critical Lennard-Jones Fluid. *Chem. Phys. Lett.* **1974**, *28* (4), 578−581.
(85) Tribello, G. A.; Bonomi, M.; Branduardi, D.; Camilloni, C.; Bussi, G. PLUMED 2: New Feathers for an Old Bird. *Comput. Phys. Commun.* **2014**, *185* (2), 604−613.
(86) Grubmüller, H.; Heymann, B.; Tavan, P. Ligand Binding: Molecular Mechanics Calculation of the Streptavidin-Biotin Rupture Force. *Science (Washington, DC, U. S.)* **1996**, *271* (5251), 997−999.
(87) Souaille, M.; Roux, B. Extension to the Weighted Histogram Analysis Method: Combining Umbrella Sampling with Free Energy Calculations. *Comput. Phys. Commun.* **2001**, *135* (1), 40−57.
(88) Kumar, S.; Rosenberg, J. M.; Bouzida, D.; Swendsen, R. H.; Kollman, P. A. THE Weighted Histogram Analysis Method for Free-Energy Calculations on Biomolecules. I. The Method. *J. Comput. Chem.* **1992**, *13* (8), 1011−1021.
(89) Grossfield, A. WHAM: The Weighted Histogram Analysis Method, Version 2.09. http://membrane.urmc.rochester.edu/content/wham/, 2015.
(90) Bailleul, S.; Rogge, S. M. J.; Vanduyfhuys, L.; Van Speybroeck, V. Insight into the Role of Water on the Methylation of Hexamethylbenzene in H-SAPO-34 from First Principle Molecular Dynamics Simulations. *ChemCatChem* **2019**, *11*, 3993.
(91) Contreras-GarcÍa, J.; Johnson, E. R.; Keinan, S.; Chaudret, R.; Piquemal, J.-P.; Beratan, D. N.; Yang, W. NCIPLOT: A Program for Plotting Noncovalent Interaction Regions. *J. Chem. Theory Comput.* **2011**, *7* (3), 625−632.
(92) Alonso, M.; Woller, T.; Martín-Martínez, F. J.; Contreras-García, J.; Geerlings, P.; De Proft, F. Understanding the Fundamental Role of π / π, σ / σ, and σ / π Dispersion Interactions in Shaping Carbon-Based Materials. *Chem. - Eur. J.* **2014**, *20* (17), 4931−4941.
(93) Değirmenci, I.; Eren, Ş.; Aviyente, V.; De Sterck, B.; Hemelsoet, K.; Van Speybroeck, V.; Waroquier, M. Modeling the Solvent Effect on the Tacticity in the Free Radical Polymerization of Methyl Methacrylate. *Macromolecules* **2010**, *43* (13), 5602−5610.
(94) De Sterck, B.; Vaneerdeweg, R.; Du Prez, F.; Waroquier, M.; Van Speybroeck, V. Solvent Effects on Free Radical Polymerization Reactions: The Influence of Water on the Propagation Rate of Acrylamide and Methacrylamide. *Macromolecules* **2010**, *43* (2), 827−836.
(95) Furuncuŏglu Özaltn, T.; Děgirmenci, I.; Aviyente, V.; Atlgan, C.; De Sterck, B.; Van Speybroeck, V.; Waroquier, M. Controlling the Tacticity in the Polymerization of N-Isopropylacrylamide: A Computational Study. *Polymer* **2011**, *52* (24), 5503−5512.
(96) Hermosilla, L.; Catak, S.; Van Speybroeck, V.; Waroquier, M.; Vandenbergh, J.; Motmans, F.; Adriaensens, P.; Lutsen, L.; Cleij, T.; Vanderzande, D. Kinetic and Mechanistic Study on P-Quinodimethane Formation in the Sulfinyl Precursor Route for the Polymerization of Poly(p-Phenylenevinylene)(PPV). *Macromolecules* **2010**, *43* (18), 7424−7433.
(97) Değirmenci, I.; Aviyente, V.; Van Speybroeck, V.; Waroquier, M. DFT Study on the Propagation Kinetics of Free-Radical Polymerization of Alpha-Substituted Acrylates. *Macromolecules* **2009**, *42* (8), 3033−3041.
(98) Lobachevsky, S.; Schiesser, C. H.; Lin, C. Y.; Coote, M. L. First-Principles Prediction of Rate Coefficients for Free-Radical Cyclization Reactions at Selenium. *J. Phys. Chem. A* **2008**, *112* (51), 13622−13627.
(99) Lin, C. Y.; Izgorodina, E. I.; Coote, M. L. First Principles Prediction of the Propagation Rate Coefficients of Acrylic and Vinyl Esters: Are We There Yet? *Macromolecules* **2010**, *43* (1), 553−560.
(100) Vergaelen, M.; Verbraeken, B.; Monnery, B. D.; Hoogenboom, R. Sulfolane as Common Rate Accelerating Solvent for the Cationic Ring-Opening Polymerization of 2-Oxazolines. *ACS Macro Lett.* **2015**, *4* (8), 825−828.
(101) Arraez, F. J.; Xu, X.; Van Steenberge, P. H. M.; Jerca, V. V.; Hoogenboom, R.; D'Hooge, D. R. Macropropagation Rate Coefficients and Branching Levels in Cationic Ring-Opening Polymerization of 2-Ethyl-2-Oxazoline through Prediction of Size Exclusion Chromatography Data. *Macromolecules* **2019**, *52* (11), 4067−4078.
(102) Izgorodina, E. I.; Coote, M. L. Accurate Ab Initio Prediction of Propagation Rate Coefficients in Free-Radical Polymerization: Acrylonitrile and Vinyl Chloride. *Chem. Phys.* **2006**, *324* (1), 96−110.

https://dx.doi.org/10.1021/acs.macromol.0c00865
Macromolecules 2020, 53, 3832−3846